Limnol. Oceanogr., 33(2), 1988, 203–226
© 1988, by the American Society of Limnology and Oceanography, Inc.

Discoveries and testable hypotheses arising from Coastal Zone Color Scanner imagery of southern Lake Michigan[1]

C. H. Mortimer
Center for Great Lakes Studies, University of Wisconsin–Milwaukee, P.O. Box 413, Milwaukee 53201

Abstract

CZCS (Coastal Zone Color Scanner) images, confined mainly to the southern basin of Lake Michigan during the warm-up phases of 1979, 1980, and 1981, have furnished tools for synoptic reconnaissance of the wind-perturbed transition of the thermal regime in large basins from the winter to summer condition (including front formation and upwelling events), the coupling of phytoplankton growth with that transition, the intermittent mobilization and surface transport of sediment resuspended by storms, and the extensive temporary trapping of river-derived dissolved organic matter (gelbstoff) between the shoreline and the offshore-migrating thermal front. Intermittent resuspension of particles and variable inputs of gelbstoff, which occur in many coastal waters, render inapplicable the CZCS algorithms successfully used in ocean studies for atmospheric correction and for quantification of phytoplankton chlorophyll. That disappointment notwithstanding, there is a favorable match of the coverage and scene-revisit frequency of the CZCS and the space and time scales of significant features of the above-listed processes. The observed pattern changes shed new light on the above processes and generate several testable conjectures. These relate to whole-basin sediment transport, coastal upwelling of near-bottom sediment suspensions, and frontal hydrodynamics and its coupling with phytoplankton distributions.

During 8 yr of operation on the polar-orbiting satellite Nimbus-7, the Coastal Zone Color Scanner (CZCS) (Hovis 1981; Hovis et al. 1980) has scored notable successes in mapping the distributions of phytoplankton pigment and diffuse attenuation coefficient in ocean surface layers which are relatively free of suspended mineral sediment (Smith and Baker 1982; Gordon and Morel 1983; Abbott and Zion 1985; Brown et al. 1985; *see also* Gower 1981). The work reported here was initially undertaken in the hope that CZCS images, after application of the algorithms developed for marine studies, would yield similar synoptic insights into dynamics of phytoplankton production in Lake Michigan and in coastal waters generally. A quantitative outcome, however, proved elusive because mineral turbidity arising from intermittent sediment resuspension introduced frequent ambiguities into the interpretation. This problem was also encountered elsewhere (Walters and Schumann 1985). Resolution of those ambiguities awaits appropriate combinations of remote and in situ measurements with optical modeling. Nevertheless, Lake Michigan images have revealed previously unknown features of the development and wind-perturbation of the spring thermocline and have thrown new light on patterns of sediment transport and phytoplankton distribution. Interpretations of those patterns have generated new questions which invite testing.

The results here presented are restricted to the southern half of Lake Michigan and to the April–June transition from the winter condition of nearly complete mixing to the onset of whole-basin summer stratification. Basin characteristics, thermocline development, and image handling procedures are outlined, and the images are reviewed after partitioning into three sections, each representing a different wind regime: 6 weeks of weak wind, April–May 1979, with no major resuspension; 1980 and 1981 storms with consequent resuspension events; and upwelling episodes associated with northerly wind in June 1979 and 1980. Implications for other coastal waters, which contain significant quantities of mineral particles and dissolved organic matter, are considered in the concluding discussion.

This work was largely dependent on the access which W. Hovis and colleagues at the

[1] Contribution 290, Center for Great Lakes Studies. This work was supported mainly by grant NAG 5-209 SI from NASA and partially by grant NA 81 RA C00130 from NOAA, Great Lakes Environmental Research Laboratory, Ann Arbor, Michigan.

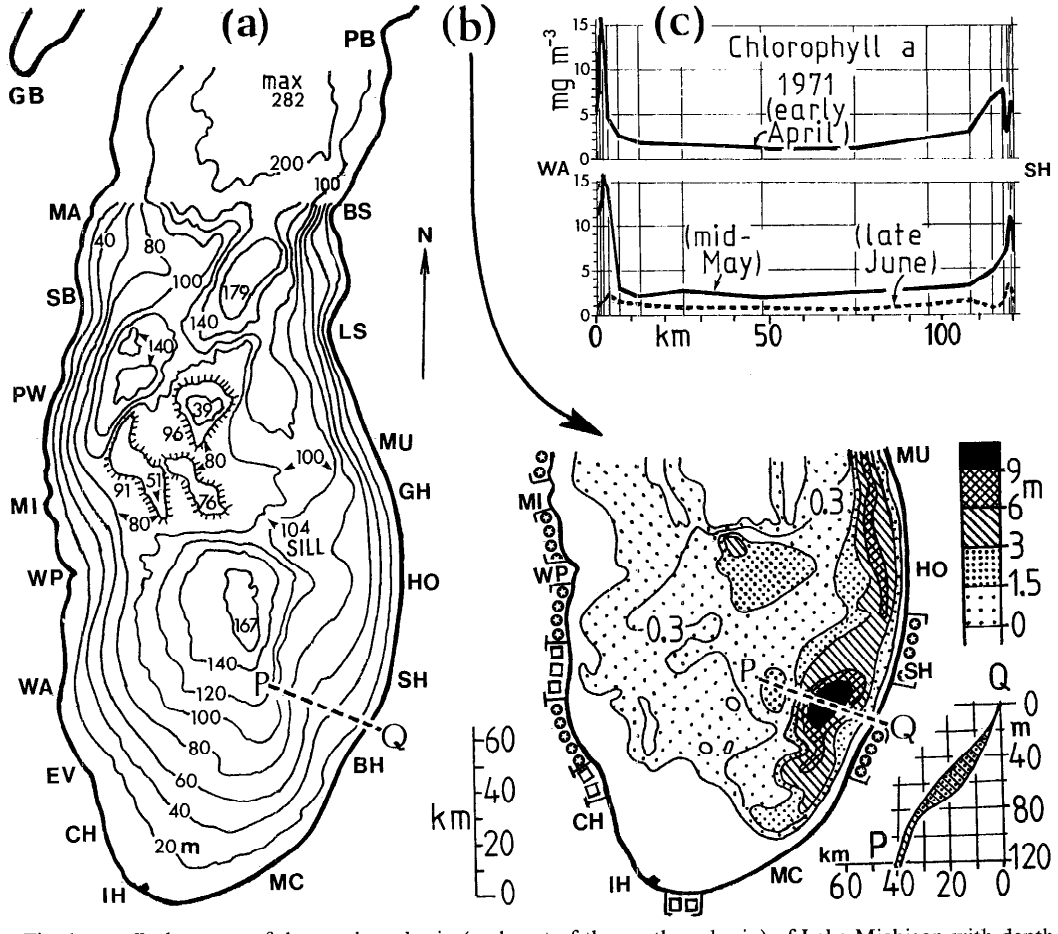

Fig. 1. a. Bathymetry of the southern basin (and part of the northern basin) of Lake Michigan with depth contours at 20-m intervals, showing sills at 91 and 104 m and elevations with summits at 39, 51 and 76 m below the surface (source, U.S. Lake Survey Chart). The line PQ defines the section illustrated in Fig. 13. The letter code, used throughout the text, designates place names in counterclockwise order. GB—Green Bay; MA—Manitowoc; SB—Sheboygan; PW—Port Washington; MI—Milwaukee; WP—Wind Point, Racine; WA—Waukegan; EV—Evanston; CH—Chicago; IH—Indiana Harbor; MC—Michigan City; BH—Benton Harbor; SH—South Haven; HO—Holland; GH—Grand Haven; MU—Muskegon; LS—Little Sable Point; BS—Big Sable Point; PB—Point Betsie.

b. Thickness contours (m) of the uppermost (Waukegan) sediment layer surveyed by Lineback and Gross (1972). Also shown, the sediment distribution in the vertical section PQ and shoreline characteristics (from Great Lakes Basin Comm. 1975): circled stars—potentially erodible high and low bluffs; squares—"erodible low plains"; blank stretches—not normally erodible, comprising rock, sand dunes, wetlands, seawall protection, and "noncrodible low plains."

c. Surface Chl *a* concentration in the WA to SH transect of Lake Michigan during spring 1971 (redrawn from Tarapchak and Stoermer 1976). Vertical lines indicate sample locations.

Environmental Satellite Service of NOAA gave me to their collection of CZCS transparencies and tapes (some also supplied by NASA) and on their assistance with image processing. This paper has also had the benefit of comments from R. P. Bukata, W. A. Hovis, and anonymous reviewers.

Basin characteristics

The southern basin of Lake Michigan (Fig. 1a: 300 km long, 130 km max width, 167 m max depth) is bounded to the north by three elevated features and is connected to the deeper northern basin over eastern and

western sills of respective depths 104 and 91 m. (For brevity, place-names are indicated throughout by the codes listed in the legend to Fig. 1.) The basin shape is relatively symmetrical about the central deep, but in two important respects it is remarkably *asymmetrical.* First, the maximum thickness of the postglacially consolidated sediment (the Waukegan stratum mapped by Lineback and Gross 1972) is encountered, not in the central deep, but offset to lie along the eastern slope (Fig. 1b). Commonly above that bank of sediment is a bottom layer of turbid water a few meters thick, named the nepheloid layer by its discoverers (Chambers and Eadie 1981).

The second asymmetry is that of shoreline composition (Fig. 1b). The western and eastern shorelines differ, in that the former includes a much greater proportion of narrow beaches and potentially erodible bluffs (Great Lakes Basin Comm. 1975, their figures 12–19) while the latter is characterized by long stretches of wide sand beaches backed by dunes. Much of the southern shoreline is protected by manmade structures. The percentages of shoreline designated as "potentially erodible" in the western (SB–EV), southern (EV–BH), and eastern (BH–LS) sectors are 92, 6, and 38, respectively. Large areas of the lakebed along the west and south shore and on the shallow elevations to the north are devoid of recent, permanent, fine-grained sediment. Materials which settle there during calm weather are resuspended by waves and currents during the next storm. The principal, present-day external sources of sediment are rivers, entering mainly along the eastern sector, and shore erosion along the western sector.

After each resuspension event, the coarser sediment fractions settle quickly, leaving the finer particles to be transported in circulation patterns as yet poorly understood. Unstratified circulation models (e.g. that of Murty and Rao 1970) predict a counterclockwise gyre as the response to steady S–SW winds over the southern basin, but the variability of real winds ensures that steady state conditions are rarely approached. Large day-to-day variations in local circulation patterns arise from changes in wind stress, from currents driven by large-scale topographic Rossby waves (Saylor et al. 1980), and, during the stratified season, by a variety of internal motions (Mortimer 1971). This complexity notwithstanding, the sediment transport paths revealed in later figures and in the depositional pattern shown in Fig. 1b suggest that a prominent feature of the long-term average circulation pattern in the southern basin is a counterclockwise gyre with a relatively quiescent "core" lying to the east of basin center. The (1976) circulation model of Allender, driven by the climatologic average wind for April, reproduced just such a pattern.

Spring thermocline evolution

First described by Tikhomirov (1963) for Lake Ladoga and by Rodgers (1966) for Lake Ontario, the spring warm-up starts with a near-isothermal (winter) basin at a temperature near 2°C, i.e. below the temperature of maximum density. Warming and stratification begins in April in shallow, nearshore water where the isotherms assume the wedge pattern illustrated in Bennett's (1971) model (Fig. 2). A front, or "thermal bar," marked by a nearly vertical 4°C isotherm, separates offshore unstratified water at $<4°$ from inshore stratified water at $>4°$. As the season advances, the shore-hugging band of stratified water warms and widens, encroaching progressively on the central cold, unstratified pool. The offshore-directed pressure gradient force P, created by tilting of the isopycnals, drives a geostrophic current G, the speed and alongshore counterclockwise progress of which is such that the resulting onshore-directed Coriolis force C exactly opposes force P. As solar heat input continues, the front advances progressively away from shore, leaving stratified water on the inshore side. The behavior of this spring thermocline in Lake Ontario was described by Csanady (1974).

It has been generally assumed that the spring thermocline will behave similarly in Lake Michigan; but the evidence is surprisingly fragmentary and confined to single locations or sections, for example, the pioneering temperature surveys of Church (1945), Noble et al. (1968), and the study of phytoplankton and temperature distribution off GH by Stoermer (1968). The

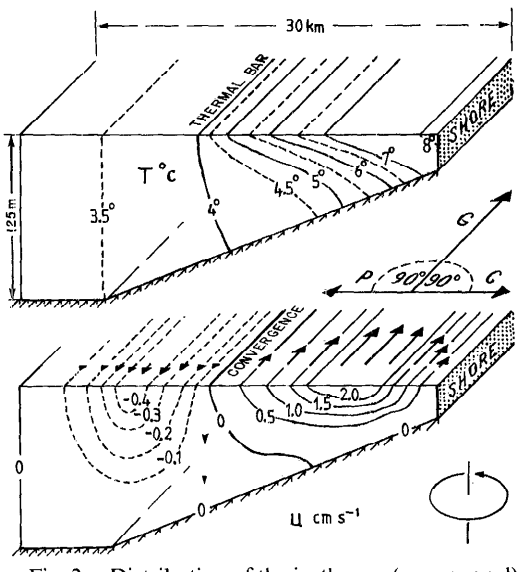

Fig. 2. Distribution of the isotherms (upper panel) and geostrophic current (lower panel) in a section normal to the shore, redrawn from the mathematical model of Bennett (1971) of the spring thermocline in a large lake with rotation taken into account. The distributions are those that have developed after 45 d of heat input through the surface at a uniform rate of 194 W m^{-2}, starting from initial isothermy at 2°C. The lettered diagram, illustrating geostrophic balance, is explained in the text.

CZCS images of surface temperature, here presented, provide the first synoptic whole-basin views of formation and migration of the spring thermocline front in Lake Michigan. Surprising also is the fact that published information on cross-basin distributions of near-surface chlorophyll is confined to the transects of Tarapchak and Stoermer (1976) illustrated in Fig. 1c. During the spring the highest concentrations were found close to but not at the shoreline, and nearshore and offshore concentrations were higher in April and May than in June.

The CZCS images and their treatment

Specifically designed to encompass the low reflectance range of ocean waters and to avoid sunglint, the sensor sensitivity, spectral coverage, and scene-revisit frequency of the CZCS make it more suitable than Landsat for exploration of color changes in coastal waters. But that high sensitivity exacts a price, i.e. the need to remove or account for significant and sometimes dominant radiance contributions from Rayleigh and aerosol scattering in the atmosphere. Those contributions add significantly to the total radiance received in the four CZCS channels covering the visible spectrum: channel 1 (blue, 443±10 nm); channel 2 (blue-green, 520±10 nm); channel 3 (green, 550±10 nm); channel 4 (red, 670±10 nm). Channel 5, 750±50 nm in the near-infrared, serves to delineate water and land areas and is not portrayed here. Radiance in the thermal infrared (channel 6, 11.5±1 μm) can be used to estimate the surface (skin) temperature and is a guiding parameter in my later interpretation.

Details of the CZCS instrument and archiving procedures can be found elsewhere (Hovis 1981, 1984) and full descriptions of the algorithms (and assumptions) involved in atmospheric correction and chlorophyll quantification are given in various papers in *Oceanography from space* (Gower 1981) and by Gordon and Morel (1983). Several procedures for atmospheric correction were tested and compared on Great Lakes images by Tanis (1984).

Selected 2-min scenes (1,500 × 840 km) are processed by NASA to two levels. The Level-1 archive consists of selected scenes recorded as photographs of all six channels (principally useful for initial orientation) or on digital (CRT) tapes to which no atmospheric correction has been applied. In a few of the Level-1 scenes, further processed to Level-2 as photographs and as CRST tapes, the above-mentioned ocean-derived algorithms are applied to display the near-surface distributions of pigment concentration (chlorophyll *a* plus pheophytin) and diffuse attenuation coefficient, i.e. the products which the CZCS was designed to provide. Atmosphere-corrected radiances in channels 1 and 2 and the Rayleigh-corrected channel 4 radiance are also imaged.

The scenes assembled in later figures were mainly derived from Level-1 digital tapes. The respectively high and low reflectance ranges from land and water were treated separately. Maximum contrast was achieved by "stretching" the water radiance ranges to occupy most of the image processor's digital span (0–255 counts). The stretched scene was then photographed with its correspond-

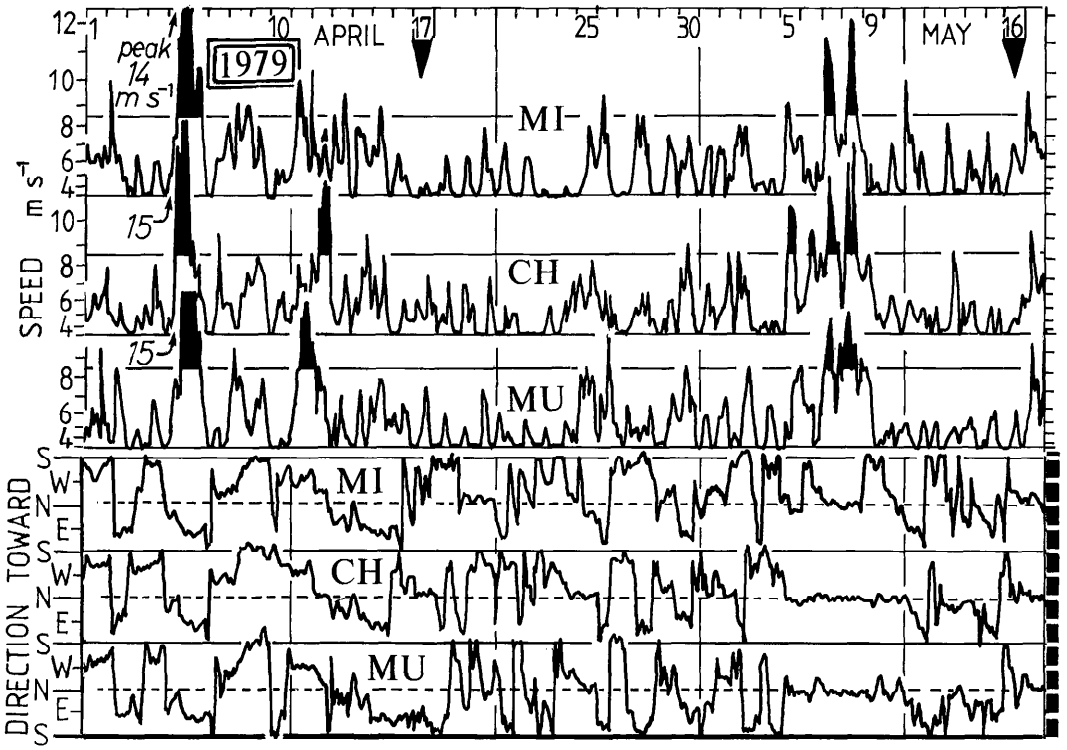

Fig. 3. Three-hourly observations of wind speed and direction at MI (Milwaukee, Mitchell Airfield), CH (Chicago, Midway Airport), and MU (Muskegon Airport), 1 April–17 May 1979. The ordinate spacing simulates stress (square of velocity >2.5 m s^{-1}), but units are given in m s $^{-1}$. Peaks >8 m s^{-1} are blackened. The down-pointing arrowheads correspond to images in Fig. 4.

ing gray scale and digital count limits. The amount of stretching was similar but not identical in each scene. Because the emphasis here is on qualitative pattern changes and because no atmospheric correction was possible, I made no attempt to derive quantitative information from the gray scales. An exception was surface temperature (channel 6), for which I used an unpublished calibration curve supplied by W. Hovis, making no correction for water content of the atmosphere. The error in this procedure cannot be judged with precision, but I have assumed a range of about ± 1°C.

For present qualitative comparisons it was not necessary to transform the tape-derived images onto a standard geographic projection. The N–S (354 km) line between the SW entrance to Sturgeon Bay (Sherwood Point) and the NW corner of Indiana Harbor was used to align the figures and to provide an approximate N–S scale. Approximate E–W scaling was obtained from the MI to MU (127 km) image distance, which varied with the obliqueness of the viewing angle. Because the satellite track is directed about 16° W of N over Lake Michigan, both N–S and E–W scales vary over the scene, but that variation is acceptable for present discussion.

An example of relatively unperturbed evolution of the thermal front (mid-April to late May 1979) with coastal trapping of dissolved organic carbon (gelbstoff)

A key variable in interpretation of the images which follow is wind stress on the basin surface. An approximate representation of that stress is obtained from 3-h records of wind speed and direction at three coastal airports (MI, CH, MU). In Fig. 3 and later figures, ordinate spacing is made proportional to speed squared (approxi-

mately proportional to stress), but actual speeds are given in m s $^{-1}$. Speeds <2.5 m s^{-1} are ignored; and peaks >8 m s^{-1} are filled in black. The choice of 8 m s^{-1} is arbitrary, but it is near the speed at which whitecaps appear and drag increases. To display the direction as well as the magnitude of the stress, I indicate the direction *toward* which the wind blows. As will become evident, the basin response is particularly sensitive to south-directed stress events. Such events (none seen in Fig. 3) are marked by black squares in later wind diagrams.

After a strong impulse toward east on 5 April 1979 and weaker pulses toward west on 11 and 12 April, winds remained weak for the rest of that month. The obliquely viewed CZCS channel 6 scene from 17 April (Fig. 4a) shows a narrow strip of warm water (average width about 4 km, at about 8°C at the surface inshore and 3° offshore) wrapped around the whole shoreline from SB to BS. It represents an early stage in the development of the front and circumshore stratification. North of SB and BS, the warm strip had not yet formed or was too narrow to be seen. Broadening of the strip to the south (surface temperature near 10°C) was perhaps a consequence of the 5 April storm. The orientation of the frontal eddies between BH and SH are consistent with a north-going geostrophic current inshore of the front, i.e. with the "backward-breaking" eddies in Griffiths and Linden's (1981) physical model of instability at the frontal edge of a buoyancy-driven coastal current.

Of the four CZCS images in the visible range, only those from channels 2 (blue-green), 3 (green), and 4 (red) are illustrated in Fig. 4a. The image from channel 1 was a paler version of that from channel 2. Remarkable is the spatial concurrence, around the southern half of the basin, of the bands of higher reflectance in channels 2, 3, and 4 and the pattern of highest surface temperature in channel 6. That concurrence even extends to shapes and locations of the frontal eddies.

Atmospheric correction of CZCS oceanic images is based on the justifiable assumption that, there, reflectance in the red channel 4 is entirely derived from the atmosphere. But, in the 17 April and later-illustrated channel 4 images from Lake Michigan, water-derived patterns are clearly recognizable and usually readily distinguishable from the diffuse atmospheric aerosol patterns, if present. The conclusion is, therefore, that the standard procedure for atmospheric correction (Gordon and Morel 1983) cannot be applied to the Great Lakes or to many coastal scenes, although ways around this difficulty can sometimes be found (Sturm 1982; Tanis 1984; and procedures reviewed by Gordon and Morel 1983).

Because winds had been weak since 12 April, it is unlikely that mineral turbidity was a major contributor to the reflectant and evidently water-derived patterns nearshore in Fig. 4a. Those patterns in scenes 2 to 4 are most probably attributable to a near-surface bloom of phytoplankton, predominantly of diatoms, in the recently stratified band of onshore water. Diatoms are commonly browner than other species, because they contain more carotenoid pigment and may also store fat. The inference, yet to be tested, is that diatoms contribute significantly to reflectance in channel 4.

The month following 17 April was one of very weak winds, except for N-directed pulses on 7 and 8 May. On 16 May (Fig. 4b) the channel 6 scene discloses a darker band of warm water, near 13°C at the surface and presumably stratified below, extending along 200 km of the east shore. Remarkably constant in width (about 10 km at MC, 8 km at MU, narrower north of LS), that band displays a distinct, nearly straight, shore-parallel front. It contrasts with the wider, cooler band (near 10°) along the west shore with its convoluted outer edge. Such

→

Fig. 4. CZCS Level-1 images illustrating early evolution of the spring fronts in southern Lake Michigan: a—channels 6, 2, 3, and 4 for 17 April 1979 (orbit 2425, start 163841 GMT); b—channels 6, 1, 2, 3, and 4 for 16 May 1979 (orbit 2826, start 165920 GMT). These and later scenes, prepared from digital tapes, were contrast-enhanced as described in the text. Where needed, the shoreline has been sketched in.

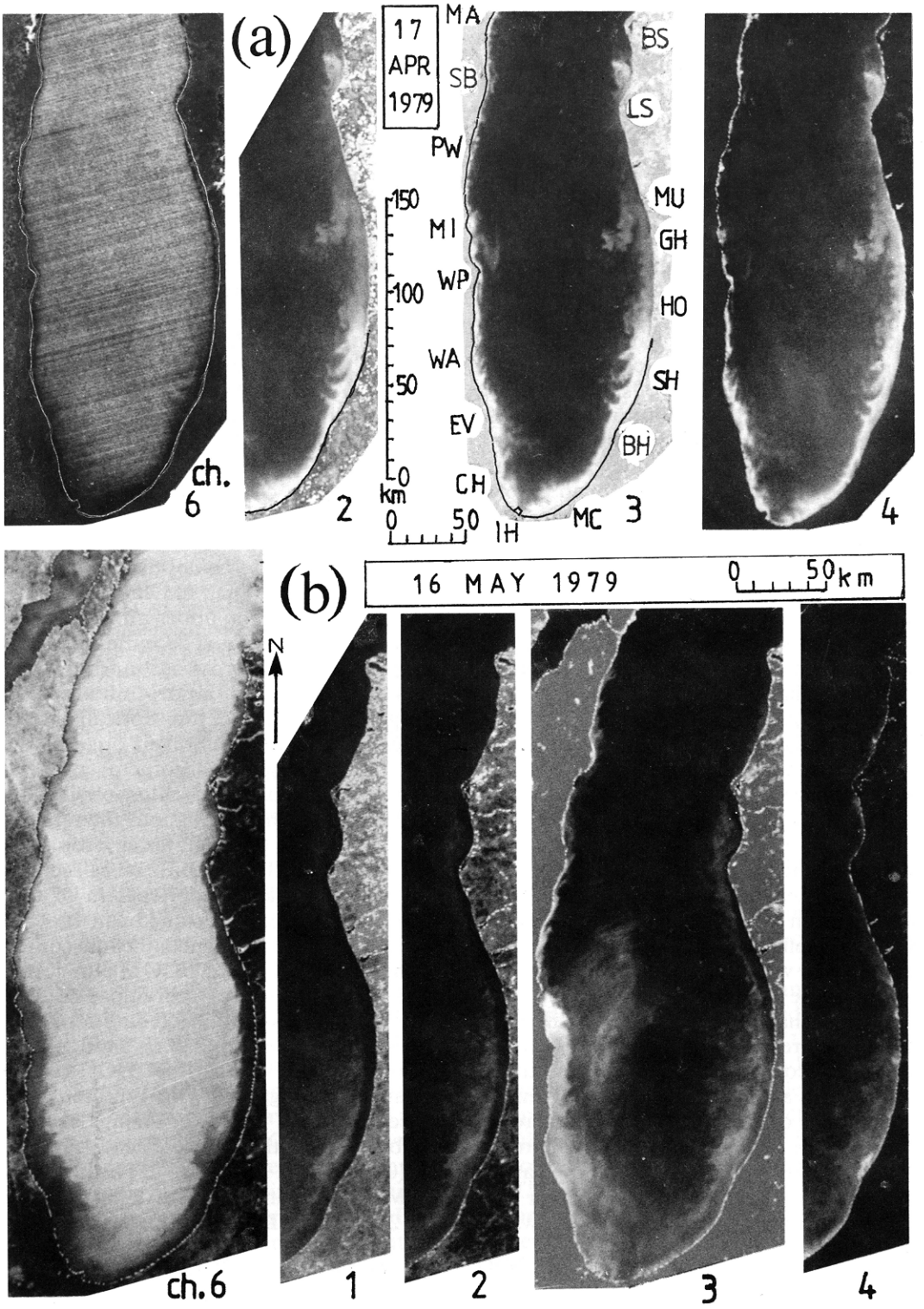
(a)
17
APR
1979
MA
SB
PW
MI
WP
WA
EV
CH
IH
MC
BS
LS
MU
GH
HO
SH
BH
150
100
50
0
km
0 50
ch.
6
2
3
4
(b)
16 MAY 1979
0 50 km
N
ch.6
1
2
3
4

cross-basin differences in surface temperature pattern, often seen in other images, can be attributed to the generally N-directed wind from 7 to 16 May. Combining with the Coriolis force, that wind pressed the stratified water against the shore along the east side, while inducing more offshore movement and frontal instability with large accompanying eddies along the west side. The relatively regular serration of the eddies along that front is reminiscent in scale and form of the pattern of baroclinic instability interpreted by Rao and Doughty (1981). Along the east shore, the straight line of the front is broken only by a convoluted area of warm water extending offshore near BH. The channel 6 estimate of midlake surface temperature on 16 May was near 4°C.

Scenes from all four visible channels are presented for 16 May (Fig. 4b) to display the diagnostic characteristics of the remarkable feature that appears along the east coast at that time of year. The feature in question is a distinct band of reduced reflectance—called the "dark alongshore band" (DAB)—extending 200 km or more along the east (but not the west) shoreline. The DAB is distinct in channels 1 and 2, less so in channel 3, and not visible in channel 4. On 16 May the offshore edge of the DAB coincided closely with the temperature front (channel 6), and early signs of a developing DAB can also be made out on 17 April (Fig. 4a, channels 2 and 3, but not 4) as an extremely narrow onshore strip between SH and MU. No such DAB was visible along the west shoreline on either date. On 16 May the nearshore reflectance patterns were partially obscured by what appeared to be diffuse haze covering the SW sector of the basin, illustrated for channel 3 only in Fig. 4b. Some water features could nevertheless be made out. They coincided in form and locations with eddies along the temperature front. In the absence of evidence for sediment resuspension, the high reflectance nearshore between MI and WP, and extending farther south, is attributable mainly to higher phytoplankton populations in surface waters there.

Because of the presence of the DAB, maximum reflectance along the east coast in channels 1 to 3 occurred, not at the shoreline, but along and just offshore of the temperature front. It was at first tempting to explain this distribution as a consequence of phytoplankton growth kinetics, characterized by initial acceleration of nearshore growth when stratification commenced, later nutrient starvation in surface layers between front and shore, and consequent confinement of maximum growth to the near-frontal region in which entrainment of nutrient-rich offshore water was in progress. That sequence appeared plausible in the light of Fig. 1c, Scavia and Bennett's (1980) verification of a Lake Ontario phytoplankton growth model, and Pingree's (1984) concept of growth stimulation at fronts in the NE Atlantic. A sequence of this kind may be operating in Lake Michigan, but it fails to explain why the DAB is seen only along the east (never along the west) shore, or why it appears only in channel 1 to 3 scenes, but not in channel 4.

In the search for clues leading to an explanation, I turned to an optical model that Bukata et al. (1985) had matched to the optical properties of the upper mixed layer in western Lake Ontario. The building blocks of that model were cross-sections of experimentally determined absorption and scattering (410–690 nm) of four optically active components: water, dissolved organic carbon (DOC), suspended mineral particles (SM), and phytoplankton chlorophyll (Chl). (In that model and throughout the remainder of this paper Chl denotes chlorophyll *a* plus pheophytin.) With those cross-sections as building blocks, model spectra of subsurface irradiance reflectance can be constructed for various concentration combinations of Chl, SM, and DOC in pure water. Thus, the influence of individual components (under Lake Ontario conditions) can be assessed. For example, Fig. 5a illustrates the influence of 2 g m^{-3} of DOC (which Bukata et al. regarded as a representative concentration in the lower Great Lakes) in combination with three concentrations of Chl (0.05, 1, and 10 mg m^{-3}). The influence of SM, in combination with 1 mg m^{-3} Chl and 2 g m^{-3} of DOC, is illustrated in Fig. 5b.

Several conclusions, discussed by Bukata et al., are relevant to Lake Michigan, but my purpose here is to use the model to discover whether there are particular realistic

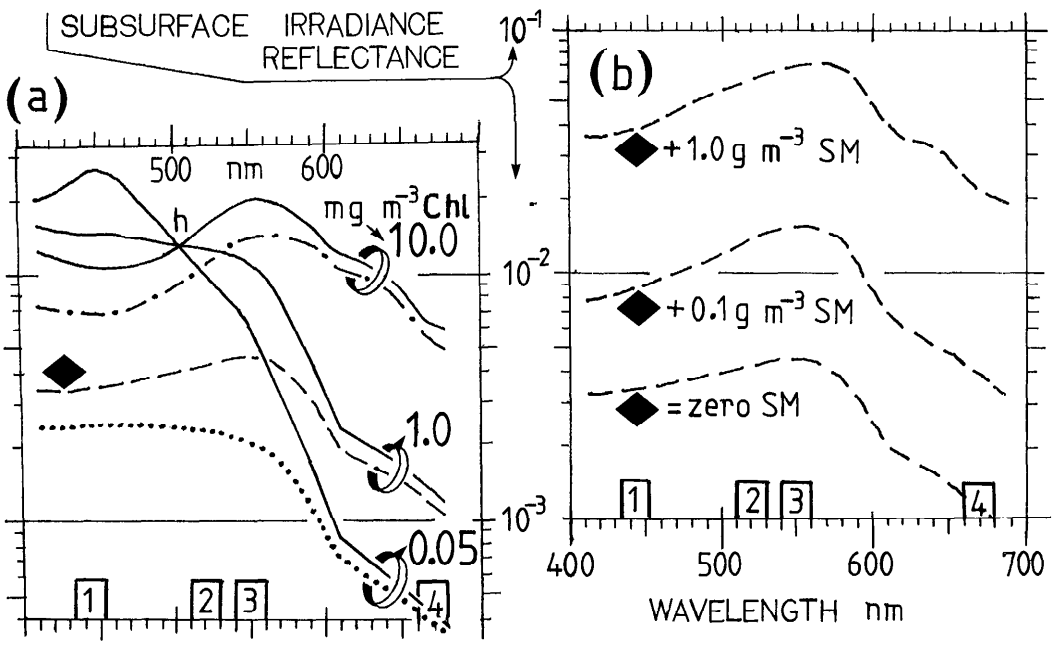

Fig. 5. Spectra of subsurface irradiance reflectance constructed by Bukata et al. (1985) from a four-component model matched to observed conditions in Lake Ontario. The components are water, Chl (chlorophyll *a* + phcophytin), SM (suspended mineral particles), and DOC (dissolved organic carbon). The spectra are here redrawn, and numbered boxes are added to indicate the wavelengths and approximate bandwidths of CZCS channels 1–4. a. With SM absent in every case, three pairs of spectra are presented for three Chl concentrations (10, 1, and 0.05 mg m^{-3}) with 2 g m^{-3} DOC (respectively, the dot-dashed, dashed, and dotted lines) and without DOC (i.e. with Chl alone, unbroken lines; note the crossover "hingepoint" at h). Adding DOC removes h and reduces reflectance—strongly at the blue end, weakly at the red end of the spectrum. DOC-induced reduction of blue reflectance becomes less as Chl concentration increases. b. Repeats (at bottom) the diamond-marked dashed-line spectrum in panel a for the combination: 1 mg m^{-3} Chl, 2 g m^{-3} DOC, no SM. Adding relatively small quantities of SM (0.1 and 1 g m^{-3}, illustrated by the middle and top spectra) increases reflectance fairly uniformly across the spectrum by factors near 3 at the blue and 12 at the red ends and near 4 and 16 in the green. Further model spectra, corresponding to other combinations, are illustrated in Fig. 12.

combinations of component concentrations that can reproduce the characteristic features of the DAB. To that end, a typical mid-May transect normal to the eastern shoreline was modeled as three contiguous compartments: offshore, frontal, and inshore. Each compartment was assumed to be well mixed, and to each was added a particular combination of Chl, SM, and DOC concentrations. For each compartment the corresponding reflectances were calculated at the four CZCS visible wavelengths. Examples of those calculations are presented, for frontal and inshore compartments only, in Table 1. To simulate the DAB effect, it is necessary to find combinations of Chl, SM, and DOC concentrations that produce higher reflectances frontally than inshore at the wavelengths of channels 1, 2, and 3, while at the same time permitting the frontal and inshore reflectances to be nearly the same for channel 4. Reflectance ratios in Table 1 summarize the following main conclusions from a more detailed analysis.

First, in the absence of SM and DOC, the DAB effect cannot be simulated by a higher concentration of Chl frontally than inshore (case A). Second, with Chl and DOC concentrations held at the same level in both compartments, the DAB effect cannot be simulated by maintaining the SM concentration higher frontally than inshore (case B). Third, the DAB effect can be simulated, either by making the Chl concentration higher inshore than frontally, while holding DOC at the same level in both compartments (case C), or by allowing the DOC concentration to be higher inshore than frontally (cases D, E). Of these latter alter-

Table 1. Subsurface irradiance reflectance (R) predicted for the near-frontal (F) and inshore (I) compartments of the model described in the text, when those compartments contain the indicated concentrations of chlorophyll (Chl, mg m^{-3}), suspended mineral particles (SM, g m^{-3}), and dissolved organic carbon (DOC, g m^{-3}). The reflectance predictions, at the wavelengths corresponding to CZCS channels 1–4, are derived from model spectra matched by Bukata et al. (1985) to conditions in Lake Ontario. Also tabulated, for each CZCS channel and for each selected case, is the (F:I) reflectance ratio, referred to in the text.

					Reflectance, $R \times 10^4$, in CZCS channel No.			
Case	Chl	SM	DOC		1	2	3	4
A	10	0	0	F	102	138	190	60
	5	0	0	I	110	135	170	33
				F:I	0.93	1.02	1.12	1.82
B	0.5	0.1	2	F	85	125	142	36
	0.5	0	2	I	30	33	35	8
				F:I	2.83	3.79	4.06	4.50
C	0.5	0.1	2	F	85	125	142	36
	5	0	2	I	57	84	105	36
				F:I	1.49	1.49	1.35	1.00
D	1	0.05	1	F	97	128	140	26
	1	0.05	2	I	61	86	100	25
				F:I	1.59	1.49	1.40	1.04
E	1	0.05	3	F	44	66	76	24
	0.05	0.05	10	I	19	33	40	26
				F:I	2.32	2.00	1.90	0.92

native scenarios, both of which could explain the presence of the observed DAB (Fig. 4b), the shoreward increase of Chl (case C) seems the least likely, because there is no reason to expect Chl production and distribution along the eastern and western shores to be very different (*see also Fig. 1c*). This elimination leaves case D (a shoreward increase of DOC concentration along the east coast only) as the most likely explanation of the DAB. Supporting evidence for this conclusion arises from the peculiar hydrology of Lake Michigan.

With the exception of the Fox River which flows into Green Bay, there is very little river inflow along the western shoreline. Data tabulated by the Great Lakes Basin Commission (1975, appendix 11) disclose that 41% of the annual runoff into Lake Michigan occurs during three spring months at the following average rates ($m^3\ h^{-1}\ km^{-2}$ of catchment): 46 in March, 68 in April, and 46 in May. The 250-km stretch of coastline from MC to LS (the coastline along which the DAB appears) receives inflow from the four major rivers (Muskegon, Grand, Kalamazoo, and St. Joseph) which together drain 42,500 km^2, i.e. 36% of the total catchment of the lake. A rough calculation concludes that, from 1 April to 21 May, the total volume delivered by those four rivers to that coastal stretch would be 3.07 km^3 (i.e. 30 d at a rate of 68 $m^3\ h^{-1}\ km^{-2}$ plus 21 d at a rate of 46). That volume of warm and relatively organic-rich water, if fully trapped at the surface between the shore and the thermal front 10 km offshore in late May, would correspond to a 250 × 10-km slab 1.2 m thick.

In reality, the trapping would not be total—because of vertical and horizontal entrainment at the advancing front—but much of the incoming warmer river water can be expected to be retained temporarily above the thermocline between the front and the shore. It appears reasonable (B. J. Eadie pers. comm.) to set the average inflowing DOC concentration near 10 g m^{-3}. Therefore, it is also reasonable to expect a DOC concentration of 1–2 mg m^{-3} above lake-ambient along the east (but not the west) shoreline. That amount would suffice (case D in Table 1) to produce the DAB effect. The timing of river inflow delivery is also consistent with the first appearance of the DAB near GH (Grand River mouth) in mid-April (Fig. 4a), with its full development along the whole east coast by mid-May, and with its disappearance by mid-June. Then the inflow rate has dropped sharply, and the earlier accumulation of DOC has become progressively diluted as the front moves offshore

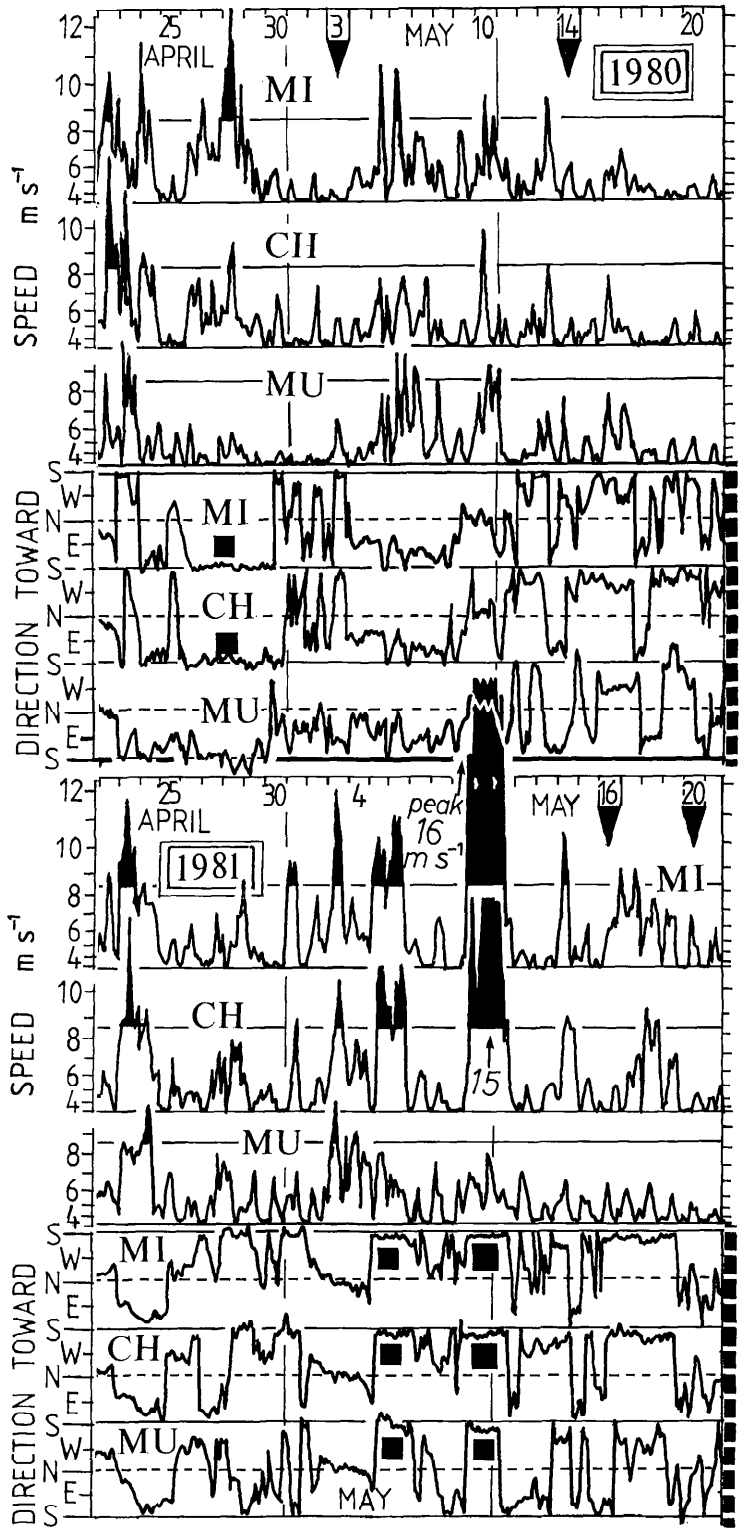

Fig. 6. As Fig. 3, but for the intervals 21 April–21 May 1980 and 1981. The CH observations are from O'Hare Airport. Sustained S-directed wind events are marked by black squares. Down-pointing arrowheads correspond to images in Figs. 7 and 8.

and breaks up. It should also be noted that the rivers deliver not only heat and DOC, but also substantial quantities of nutrients, inorganic and organic sediment, and phytoplankton chlorophyll. Those contributions and the DAB effect are not seen off the west shoreline because the river input there is much smaller.

1980 and 1981 events of extensive resuspension of sediment during strong S-directed wind stress

No major S-directed wind events occurred during April and May in 1979, but several were experienced in 1980 and 1981 (Fig. 6). Each was followed by temporary disruption of the eastern temperature front and by evidence in the CZCS images of sediment resuspension along the west shore, around the south end, and in a north-trending plume often separating from the shore near BH. Such images were also recorded by the CZCS on 5 and 18 April (neither illustrated) after storms on 31 March and 14 April. Figure 7a (3 May) records the aftermath of a similar but less violet event after 5 d of S-directed wind had peaked at 12 m s^{-1} at MI (but weaker elsewhere) on 28 April. Only images from channels 6, 1, and 3 are shown. Patterns of high reflectance in channels 2 and 4 were very similar to those in channel 3. Although the S-directed wind stress was relatively weak, it was sufficiently persistent to disrupt the front along part of the east shore (SH–LS) and, combining with the Coriolis force, to compress the western warm surface water into a narrow strip with a well-defined front along the whole of the west shoreline north of WA. Much warm surface water at about 8°C had been shifted to the southern end, and an offshore-directed warm plume was conspicuous near SH.

The band of very high reflectance around the SE corner of the basin (CH–SH) in channel 3 and, significantly, its reproduction in channel 1 reveals substantial concentration of SM, especially in the plume over the region of maximum sediment thickness near BH. On the inshore side of that plume and northward along the shore as far as MU, reflectance was reduced, presumably by an influx of dissolved organic matter as seen in 1979. The W–E scan of the CZCS, combined with the abrupt radiance change at the shoreline, complicates interpretation of one or two pixels at and immediately adjacent to the western shoreline. Nevertheless, the attribution of the high reflectance (channels 1–4) to the presence of SM rather than Chl in the narrow band along the west shoreline is justified because Chl alone would produce much lower reflectance in the blue channel.

For the remainder of May 1980 winds were very weak. Clouds obscured much of the west shore in the images from 14 May 1980 (Fig. 7b), but the south and east coasts were clear. The patterns there are reminiscent of those from 16 May 1979 (Fig. 4b). After the earlier perturbations by S-directed wind, a regular shore-parallel front had become re-established with an extensive, distinct DAB on the inshore side between BH and MU, visible in channels 1, 2, and 3, but not in 4, as in 1979. The outer edge of the DAB coincided with the temperature front between BH and MU, and the areas of highest reflectance in all the visible channels lay, as in 1979, along and just offshore of the front.

For 1981, no April scenes are illustrated. On 10–11 May occurred the most violent spring storm experienced in any of the 3 yr reviewed (Fig. 6, 16 m s^{-1} at MI, 15 m s^{-1} at CH, but only 8 m s^{-1} at MU). It blew strongly toward the S and SW for 2 d, and the resulting massive sediment resuspension is seen in Fig. 8 (16 and 20 May). Ap-

→

Fig. 7. a. CZCS Level-1 images (channels 6, 1, and 3 for 3 May 1980, orbit 7704, start 165957 GMT) illustrating a perturbation of the eastern temperature front and moderate sediment resuspension activity in southern Lake Michigan after weak but persistent S-directed winds, 28–30 April 1980. b. Partially cloud-obscured CZCS Level-1 images for 14 May 1980 (channels 6 and 1–4, orbit 7856, start 165902 GMT) illustrating a reversion to mid-May frontal formations similar to those seen in 1979 (Fig. 4b). Some retouching of the shoreline has been done. C indicates cloud.

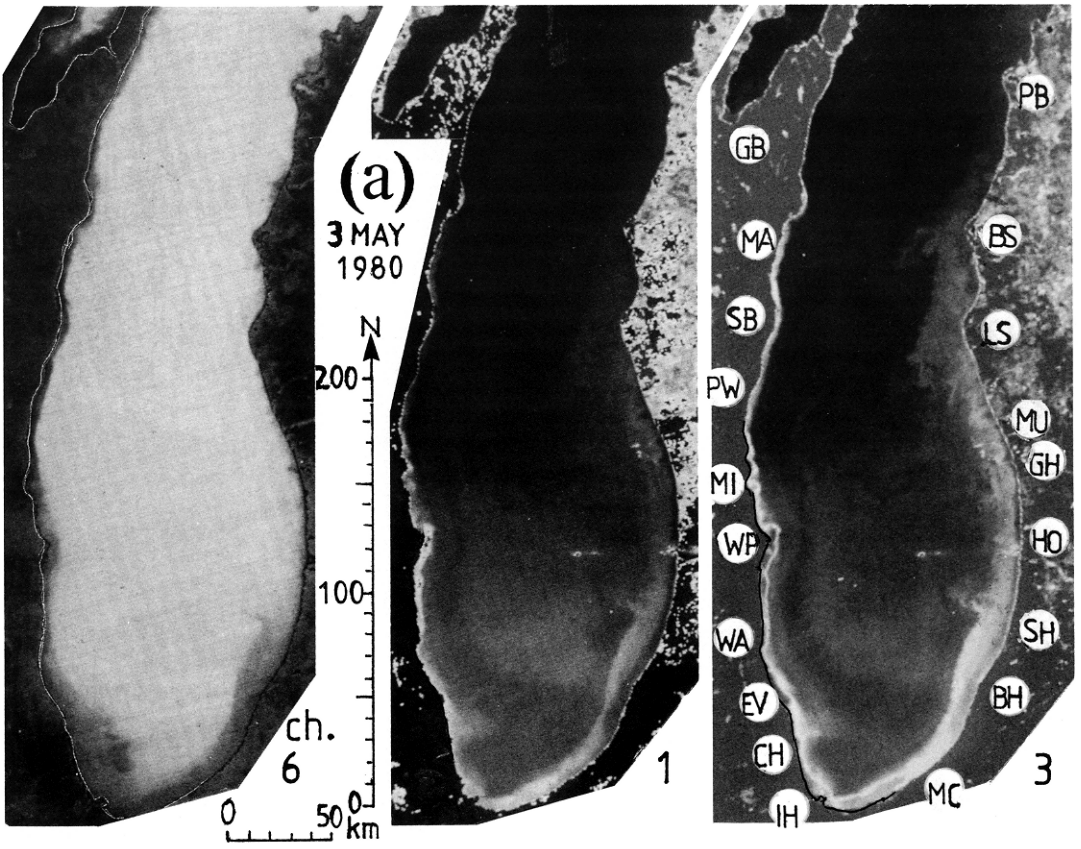
(a)
3 MAY
1980
N
200
100
0
0
50
km
ch.
6
1
3
PB
GB
MA
BS
SB
LS
PW
MU
GH
MI
HO
WP
SH
WA
BH
EV
CH
IH
MC

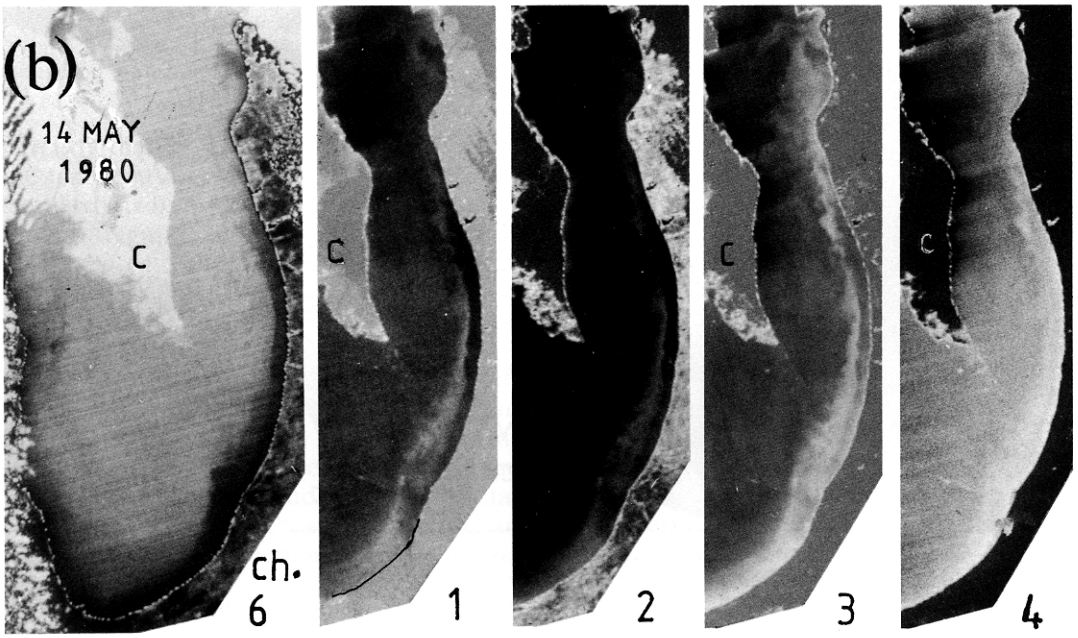
(b)
14 MAY
1980
C
ch.
6
1
2
3
4

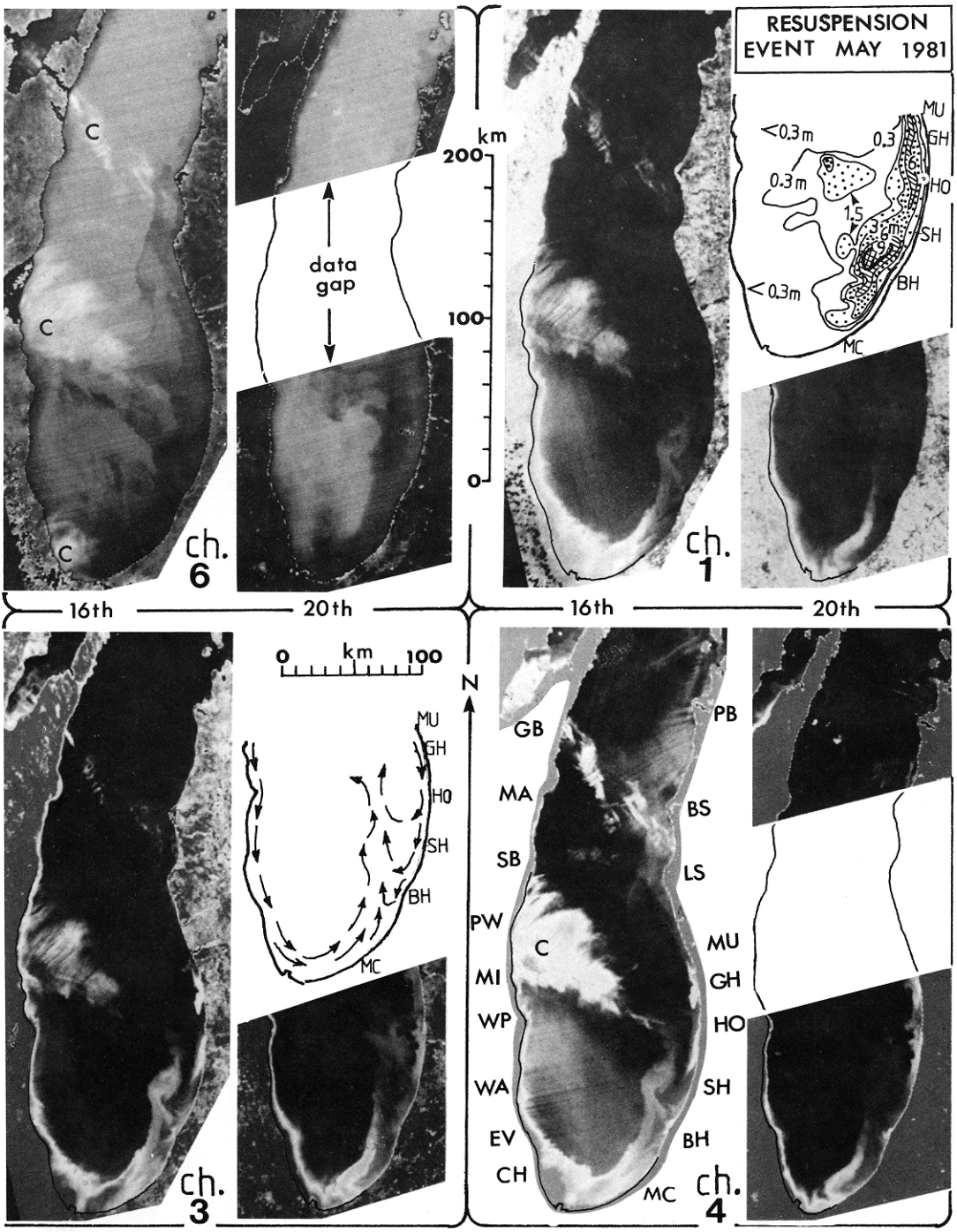

Fig. 8. A major sediment resuspension event in southern Lake Michigan illustrated by CZCS Level-1 images for 16 and 20 May 1981 (orbits 12928 and 12983, respective start times 171317 and 164337 GMT). There was a 140-km data gap on 20 May. The images are presented in 16 and 20 May pairs: above—channels 6 and 1; below—channels 3 and 4. Inset sketches illustrate sediment thickness (upper right) (from Fig. 1b) and the large-scale pattern of average surface circulation suggested by inspection of the images (lower left). In addition to the large triangular cloud C, a row of clouds extends from LS to GB, and a patch of haze extends from BS to PB.

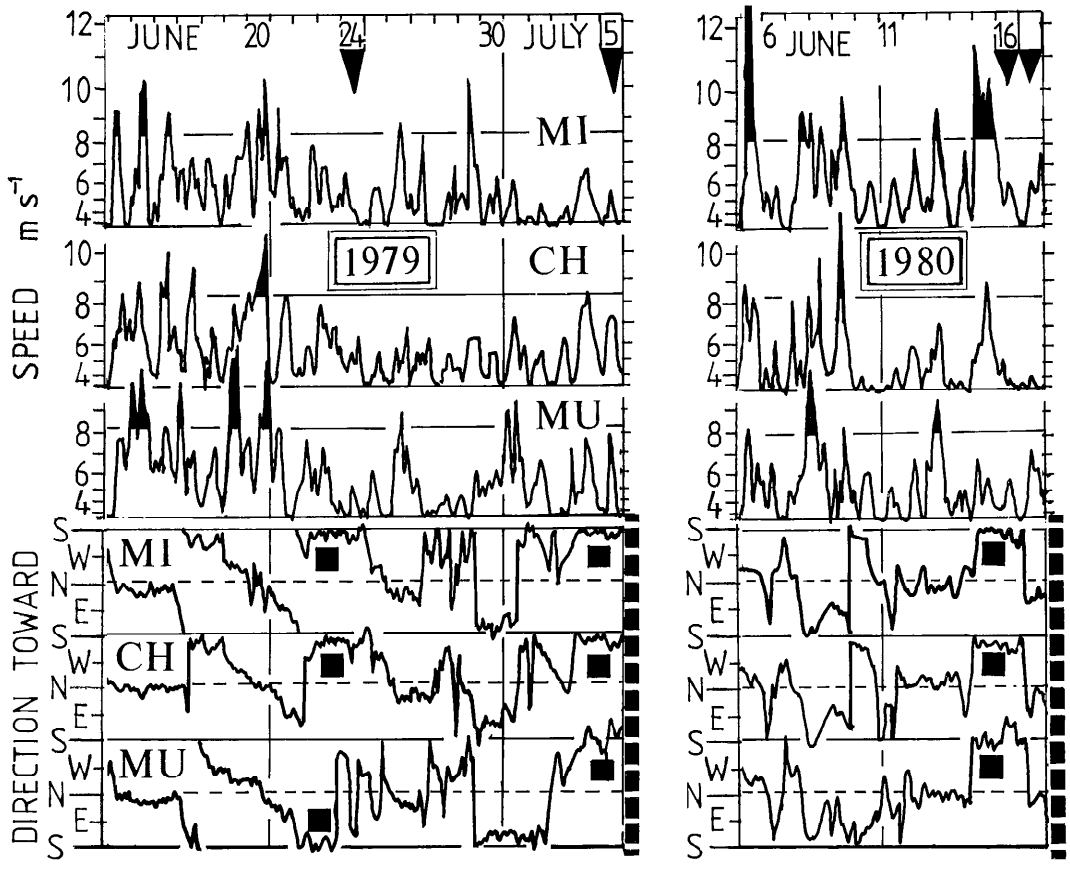

Fig. 9. As Fig. 3, but for the intervals 14 June–5 July 1979 and 5–17 June 1980 (CH 1980 observations at O'Hare). Episodes of persistent south-going winds are marked with black squares; down-pointing arrowheads correspond to images in Fig. 10.

parently that storm did not greatly disrupt the temperature front along the west shore (somewhat obscured by clouds), but the previously regular, shore-parallel front seen along the east shore on 4 May (not illustrated) had become strongly perturbed by 16 May (channel 6). There was some coastal upwelling north of HO with the creation of large plumes of warm surface water extending northwestward across most of the basin. Large quantities of warm surface water (at about 10°C) had also been moved to the south end. The DAB and the near-frontal band of high reflectance, so conspicuous in channels 1, 2, and 3 along most of the east coast in the earlier mid-May 1979 and 1980 examples, had apparently shifted farther offshore (along with the front) between MC and SH, but was dispersed north of SH.

Images from channels 1, 3, and 4 are shown for both 16 and 20 May. Those scenes (and channel 2, similar to channel 3 and not shown) are dominated by sediment resuspension. Evidence is the narrow band of very high reflectance that appeared along the whole of the west shore, which widened around the south end and merged with a north-trending plume separated from the shore near BH and marked by large streamers at its tip. By 20 May that plume had been carried farther northward by the predominantly counterclockwise circulation. Also, short highly reflectant plumes had appeared close onshore near GH and HO.

Examples of upwelling perturbations

During summer stratification, Lake Michigan is particularly responsive to a

common storm pattern, in which wind from the SW to W veers to N or NE and blows from that direction for a day or two (Mortimer 1971). The response is extensive coastal upwelling along the east shore followed by the northward progress of an internal Kelvin wave starting from the southeast corner. Similar responsiveness to S-directed and veering wind events (marked by filled squares in Fig. 9) was also revealed by CZCS imagery in June 1979 and 1980. Those winds were weak, but the response of the surface temperature field in both years was dramatic (Fig. 10).

On 24 June 1979, after several days of S-directed wind, there was an accumulation of warm surface water at about 15°C around the south end. Along the west shore the thermal front displayed a ragged appearance with gaps, whereas along the east shore it was more sharply defined, but wavy in outline. Off BH the front lay 40–50 km from shore and merged into a large, diffuse plume (first seen on 12 June, not illustrated) trending NW over the shallower plateau region to join the warm surface water on the west side. Offshore surface temperatures of large areas of the southern basin were as high as 10°C, although there were also isolated, much colder pools. From SH northward to beyond PB, the front lay between 20 and 30 km offshore. Onshore there was extensive upwelling of near-6°C water from subsurface depths. Farther south, between HO and BH, narrow strips of onshore upwelling (near 9°C) with south-trending streamers had formed. The remarkable, ropelike, braided appearance of the offshore-shifted band of warm water along the whole east coast north of BH discloses a dynamic process yet to be elucidated. A similar braided structure was seen after coastal upwelling north of LS on 16 June 1980 (Fig. 10d) when the midbasin surface temperature was about 9°C.

It is also noteworthy that by 24 June 1979 the DAB effect, so conspicuous a month earlier (Fig. 4b), had disappeared. The broad areas of moderate reflectance along the east shore in channels 2 and 4 closely matched the outline and eddy structure of the band of warm water. In the absence of strong wind events with consequent sediment resuspension during the preceding month, that moderate reflectance must be attributed mainly to phytoplankton.

A conspicuous feature in images from channels 2 and 4 on 24 June (also in channels 1 and 3 not illustrated) was a narrow onshore strip of very high reflectance extending along the whole east coastline from BH to LS. In spite of its lower sensitivity the larger scale Landsat image (Fig. 10b) also displays that strip, which appears to originate close to shore with streamers that trend SSW. Because the sites for potential erosion along that coast are limited (Fig. 1b), and because the reflecting strip in question is so extensive (200 km long) and relatively invariant in width (about 7 km), possible origins are onshore upwelling of fine sediment, which had previously settled nearshore or in river deltas, or, more probably, upwelling of deeper lying nepheloid layers. During June those layers, one may speculate, normally lie over the bank of thickest sediments deposited on the slope between BH and MU where the sedimentation rate is maximal (Edgington and Robbins 1973). Occasional upwelling of the nepheloid layer was envisaged by Bell and Eadie (1983), who described an October 1980 example.

Other CZCS scenes suggest that onshore upwelling of suspended nepheloid sediment is a fairly common occurrence along the east shore after S-directed wind. Examples are displayed in Figs. 10c, d and 8. In the latter figure, the images for channels 3 and 4 from 16 May 1981 reveal short onshore plumes of very high reflectance near HO and GH

→

Fig. 10. Illustrations of upwelling following S-directed wind events (*see Fig. 9*) in southern Lake Michigan. a. 24 June 1979; CZCS Level-1, channels 6, 2, and 4 (orbit 3365, start 170302 GMT). b. 24 June 1979; MC–MU portion of Landsat band 4 (green) image on a larger scale. c. 5 July 1979; CZCS Level-1, channel 6, and Level-2 channel 4 (orbit 3517, start 170107 GMT). d. 16 June 1980; CZCS Level-1, channel 6, and Level-2 channel 4 (orbit 8312, start 165501 GMT). The Level-2, channel 4 images are NASA-processed and Rayleigh-corrected.

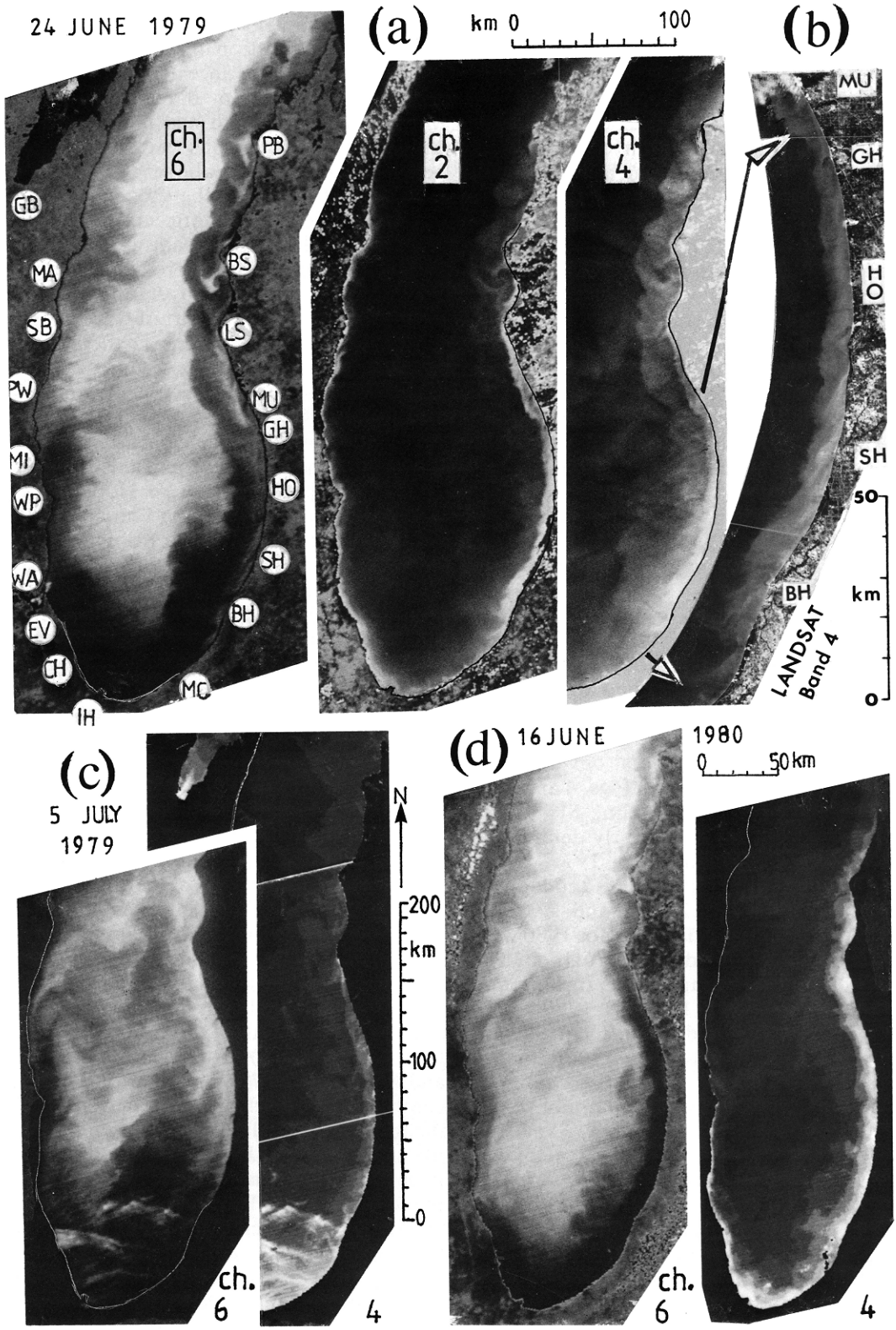
24 JUNE 1979
(a)
km 0
100
(b)
ch. 6
ch. 2
ch. 4
PB
GB
MA
BS
SB
LS
PW
MU
GH
MI
HO
WP
SH
WA
BH
EV
CH
MC
IH
MU
GH
HO
SH
BH
50
km
0
LANDSAT Band 4
(c)
5 JULY 1979
N
200
km
100
0
ch. 6
4
(d)
16 JUNE 1980
0
50 km
ch. 6
4

(i.e. near the mouths of the Kalamazoo and Grand rivers). By 20 May those plumes had expanded and coalesced into a continuous reflectant strip along the shore.

The 5 July 1979 upwelling example (Fig. 10c) marks the breakdown of the spring thermocline front (following a weak south-going wind event) and its transition to whole-basin summer stratification. The whole band of warm water north of SH had moved well away from shore and toward the south end, leaving only small warm plumes at the mouths of rivers. The offshore field was very complex with midlake surface temperatures ranging from 10° to 16°C. Although cloud-contaminated at the south end, the channel 4 image reveals a band of high reflectance along the east shore with localized small plumes of maximum reflectance emanating from that shore. A similar band appeared during the upwelling event of 16 June 1980 (Fig. 10d). In both cases upwelling of a nepheloid layer is the probable cause.

Discussion

The surface temperature patterns revealed by the CZCS shed new light on the evolution and perturbation of the spring and early summer thermocline in Lake Michigan. The sequence of frontal development during 1979 is displayed in Figs. 4 and 10a, c. Along the eastern shoreline SH to LS, where the front is most clearly defined, its average offshore distances in 1979 were 5 km on 17 April, 8 on 9 May, 8 and 9 on 16 and 21 May, 13 on 12 June, and 19 on 24 June. Corresponding distances for 1980 were 7 km on 14 May and 18 on 16 June. The trends in surface temperature, inshore and offshore as revealed by 1979–1980 CZCS images, are compared in Fig. 11 with transect data from two other years: 1942 MI to MU (Church 1945), and 1972 near WA (Commonwealth Edison Co. unpubl.). Also plotted, to demonstrate nearshore variance and upwelling events, are daily temperatures in the St. Joseph municipal water intake.

In Fig. 11, the caption of which should be consulted for details, the inshore curve (dashed line) in late March lay a little below the offshore curve (continuous line), and both were below 4°C. The higher warming rate with stratification inshore caused the curves to cross over in early April and to attain their maximum divergence in late May. By then the front had moved 10 km or more offshore, the offshore surface temperature had climbed above 4°C, and the resilience of the front/thermocline system to perturbations had noticeably lessened. During June the thermal contrast across the front became progressively reduced, and the two curves in Fig. 11 converge to meet in early July, marking the start of whole-basin summer stratification. June is therefore a transition month in which the circumshore band of stratified water becomes more vulnerable to offshore shifts and disruptions forced by upwellings. The surface temperature fields, both inshore and offshore, become more patchy (*see also* Noble et al. 1968), and large plumes and streamers of warm surface water emerge from the front and extend out across the basin, particularly over the midlake shallower area between MI and MU. Along the west shore the front is generally much more diffuse and convoluted than along the east shore, and the inshore surface temperature there is generally somewhat lower. In the northern basin (not illustrated), the central pool of cold unstratified water persists longer—until late June or early July.

The evidently complex upwelling dynamics revealed in Fig. 10a and d merits investigation. It is probable that the braided convolutions are the product of inertial motion, at and inshore of the front, which accompanies the geostrophic adjustment forced by the upwelling. Indeed, after wind reversals leading to upwelling in Lake Ontario during May 1972, inertial currents were demonstrated inshore of the "thermal bar" fronts by Csanady (1974) for the northern shore and Mortimer (1977) for the southern. The combination of circling inertial currents with the mean flow resulted in convoluted, looping current tracks. Inertial wave generation in marine fronts has also been the subject of recent research. For example, Kunze and Sanford (1984) described inertial waves with horizontal scales of order 10 km—comparable to the width of the front. Those waves are trapped and amplified and contain a large

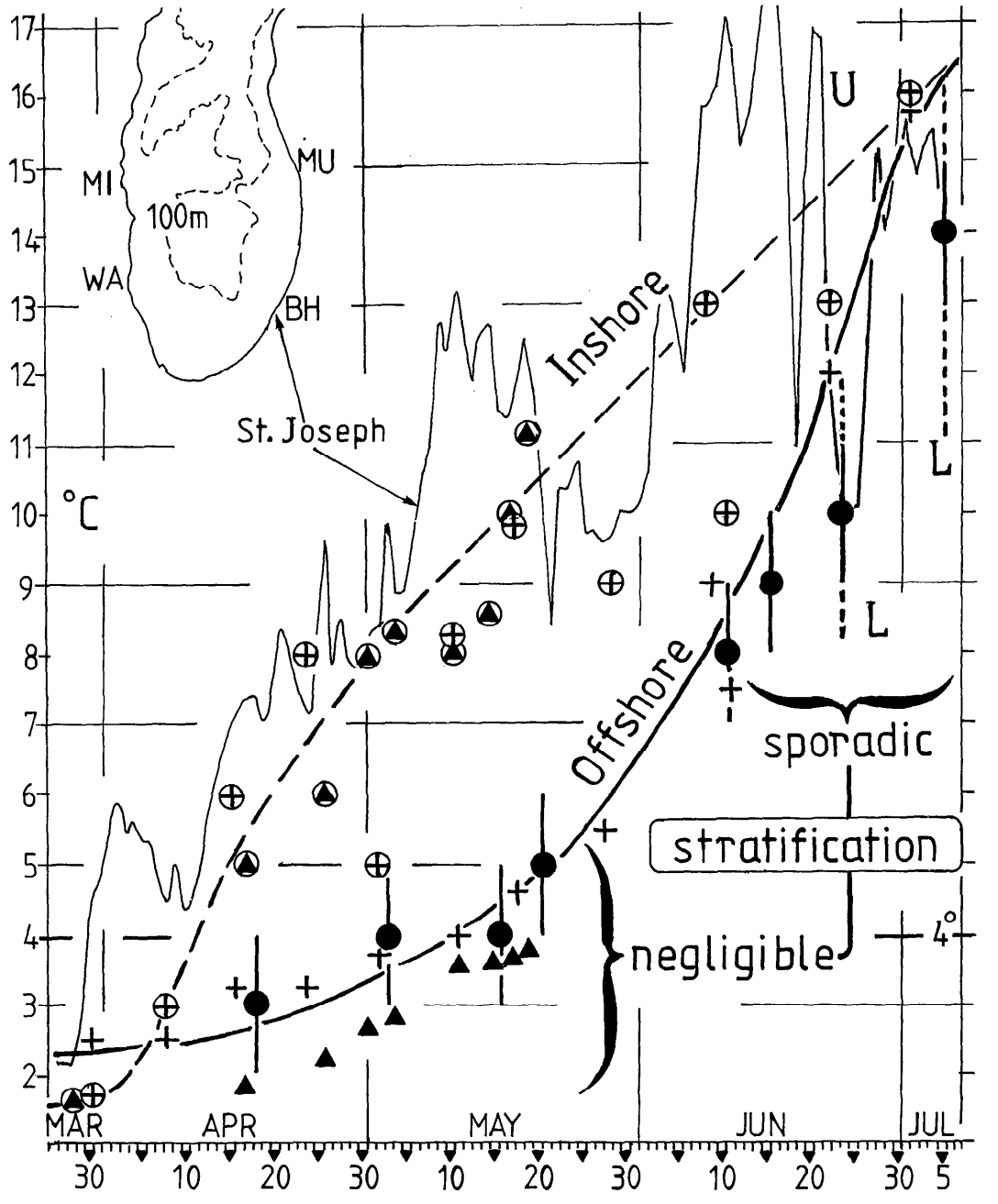

Fig. 11. Surface temperature trends from late March to early July in the southern basin of Lake Michigan: inshore trend—dashed line and circled symbols; offshore trend—continuous thick line and uncircled symbols. Also plotted, as a thin continuous line to illustrate large inshore variance and the upwelling event U, are the 1979 daily temperatures (max and min averaged) at the St. Joseph municipal water intake, 5 m deep and 1 km from shore. Eastern inshore maxima and midbasin minimum surface temperatures in the MI to MU transects of Church (1945) are indicated by circled and uncircled crosses, respectively. Filled triangles denote temperatures 10 km offshore from WA, and circled triangles denote values close inshore (1972, Commonwealth Edison Co. unpubl.). Filled circles mark the approximate 1979–1980 estimates of midbasin surface temperature from this study. The significance of the vertical "error" bars is discussed in the text. L signifies large spatial variability in offshore surface temperature.

fraction of the energy in the internal wave field and are energetic enough to play an important role in the dynamics of the front.

The CZCS scenes from the visible spectral range also yield new information and testable conjectures concerning temporary trapping of river-derived dissolved organic matter (the DAB in Figs. 4b and 7b). Similar extensive trapping of river-derived materials between front and shore along the southeastern coast of the United States was described by Blanton (1986).

New light is also shed on whole-basin sediment transport by the patterns of high reflectance in Fig. 8 and, less conspicuously, in Fig. 7a. They display storm resuspension of sediment that was deposited in shallow western and southern areas during calm weather. A band of turbid water, seen along the west coast, extends around the southern end of the basin and terminates in a plume dispersing northward from BH. It is consistent with predominant counterclockwise circulation in most of the southern part of the basin, with separation of that circulation from a much narrower circulation pattern along the east shore north of BH (as sketched in Fig. 8). The principal depositional area lies west and north of BH.

It is significant that images from CZCS channels 1–4 from all 3 yr reveal areas of high reflectance about 10–25 km offshore from BH and extending about 50 km northward during April and May. The inner boundaries of those reflectant areas lie generally at or somewhat inshore of the local temperature front. The outer boundaries, although more diffuse and convoluted, roughly fit the outer 3-m contour of sediment thickness (Fig. 1b) which marks the outer edge of the bank of thickest sediments deposited along the east slope. That edge lies about 30 km offshore near BH; it approaches to within 15 km of the shore in the north at MU; and its southern limit extends almost to MC. This distribution of reflectance suggests that there are continuing interactions between the water column and the bank of permanent sediment. One such interaction, generated by lake currents and perhaps sediment slumping with resultant gravity currents on the slope, is the formation of a near-bottom nepheloid layer discovered by Chambers and Eadie (1981). Nearshore upwelling of that layer was discussed in connection with Fig. 10.

By mid-June (Fig. 10) the thermal front has migrated to beyond 20 km offshore, thus covering the main depositional area with stratified water. The localized high reflectances then disappear. Reduction in turbulence upon stratification is the most probable explanation. Penetration of turbulence to the bottom is suppressed, and the upward pumping of finer particles ceases or is much reduced. The previously persistent reflectance from that source then disappears.

Unanswered questions concern the ultimate fate of fine particles remobilized into the surface water column by resuspension events and by the above-described turbulent interactions. How many of the particles migrate over the sills into the northern basin, and how many settle in the center of the southern basin—for example in the central patch of thickness >3 m (Fig. 1b)? How many times, on average, do particles "hop" around the basin propelled by intermittent resuspension events before they finally settle?

The Lake Michigan images also suggest that the chief challenge facing remote sensing in coastal waters is the disentanglement of the optical contributions of chlorophyll (Chl), suspended minerals (SM), and dissolved organic carbon (DOC). The nature of that challenge is demonstrated by the model spectra matched to Lake Ontario conditions illustrated in Figs. 5 and 12. The latter figure shows the effect of adding three concentrations of SM (0.1, 1, and 5 g m^{-3}) to the Chl/DOC combinations represented by the three spectra illustrated earlier in Fig. 5a. Even a small addition of SM reduces the influence of the Chl concentration on reflectance. For instance, at the blue end of the bottom spectral trio (0.1 g m^{-3} SM) that influence has been strongly suppressed. The only hope of detecting differences in chlorophyll concentration would be at the red end. For the middle spectral trio (1.0 g m^{-3} SM) the picture is reversed. Chl-related variance is least at the red end, and the brightness sequence at the blue end is the reverse of that in the bottom trio. At high concentrations of SM (5 mg m^{-3}) the spectra flatten, and the overall influence of Chl concentration is further reduced.

The complex relationships displayed in Fig. 12 may help to account for the disappointing results of an ambitious Great Lakes experiment. Coordinated by NASA-Lewis and including participants from several government, commercial, and university laboratories, the experiment was planned to include sampling from research vessels, aircraft overflights with an Ocean Color Scanner, and analysis of CZCS images, leading to algorithm development and validation. The only publications appearing to date (funding ceased in 1981) comprise Sydor's (1980) use of Landsat imagery to explore the distribution of three classes of particles suspended in Lake Superior and Tanis's (1984) development of an atmospheric correction algorithm for CZCS images. From these he then constructed color-coded maps of surface temperature and Chl and SM concentrations in all the Great Lakes on 11 June 1980. Those maps were based on an empirical optical model, derived from a disappointingly small set of ground-truth measurements, based on only 11 "standard" water samples from four lakes, including two samples only from Lake Michigan. Recently, Lathrop and Lillesand (1986) have established correlations (also empirical) between the 18 July 1984 radiances in Landsat thematic mapper bands 1–4 and same-day, near-surface measurements of chlorophyll and suspended solid concentrations and Secchi depth readings in Green Bay and Lake Michigan. It is significant that the Green Bay model predictors did not apply to Lake Michigan waters and vice versa.

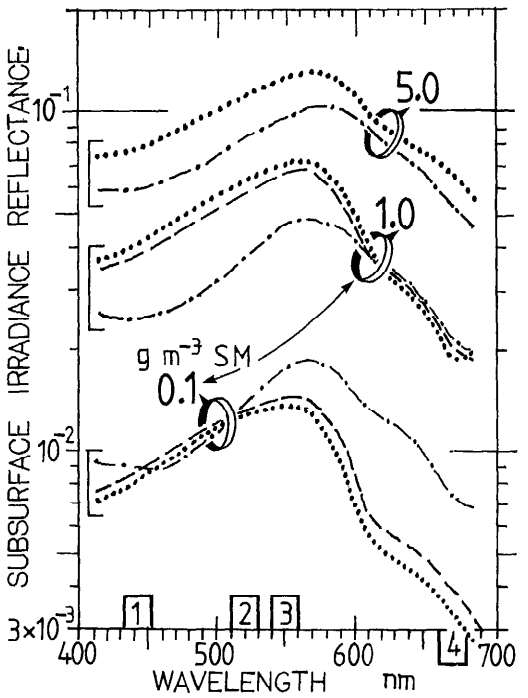

Fig. 12. Model spectra of subsurface irradiance reflectance redrawn from Bukata et al. (1985) to illustrate the effect of adding three concentrations of suspended mineral particles (SM) to three concentrations of Chl, while holding the DOC concentration at 2 g m^{-3} in every case. The three spectral groups correspond to SM additions of 5, 1, and 0.1 g m^{-3}. In each group the dotted, dashed, and dash-dotted lines refer to the Chl concentration levels 0.05, 1, and 10 mg m^{-3}. The spectral trio corresponding to zero SM is illustrated in Fig. 5a, the legend of which should be consulted for details. Numbered boxes locate the wavelengths and approximate bandwidths of CZCS channels 1–4.

This discussion and the results presented earlier lead to the conclusion that simultaneous presence of Chl, SM, and DOC in many coastal waters is the central barrier to development of universal as opposed to local, empirically derived algorithms for full exploitation of remote sensing as a quantitative tool. A review of promising ways to circumvent that barrier would be out of place here, but some possible developments can be noted: more spectral channels (including some in the near-infrared) planned for future satellite-borne instruments; atmospheric correction schemes applicable to SM estimation (Sturm 1982); laser-induced fluorescence for Chl and DOC estimation; exploitation of the specific properties of Chl, for example sun-induced fluorescence at 685 nm (Gower 1984; Topliss and Platt 1986); and systematic comparisons of the pattern features and underlying dynamics in many coastal waters, for example the evident parallels between frontal features in Lake Michigan and on ocean coasts (Walters and Schumann 1985; Blanton 1986) or in the Baltic Sea (Horstmann 1983).

Finally, to stimulate future research, some testable conjectures suggested by this study are summarized in Fig. 13. The three columns of sketches respectively portray anticipated conditions (extrapolated from CZCS surface imagery) in mid-April, mid-May, and mid-June in a transect (PQ in Fig. 1b) normal to the shore near BH. That transect, extending 40 km out to 80-m depth,

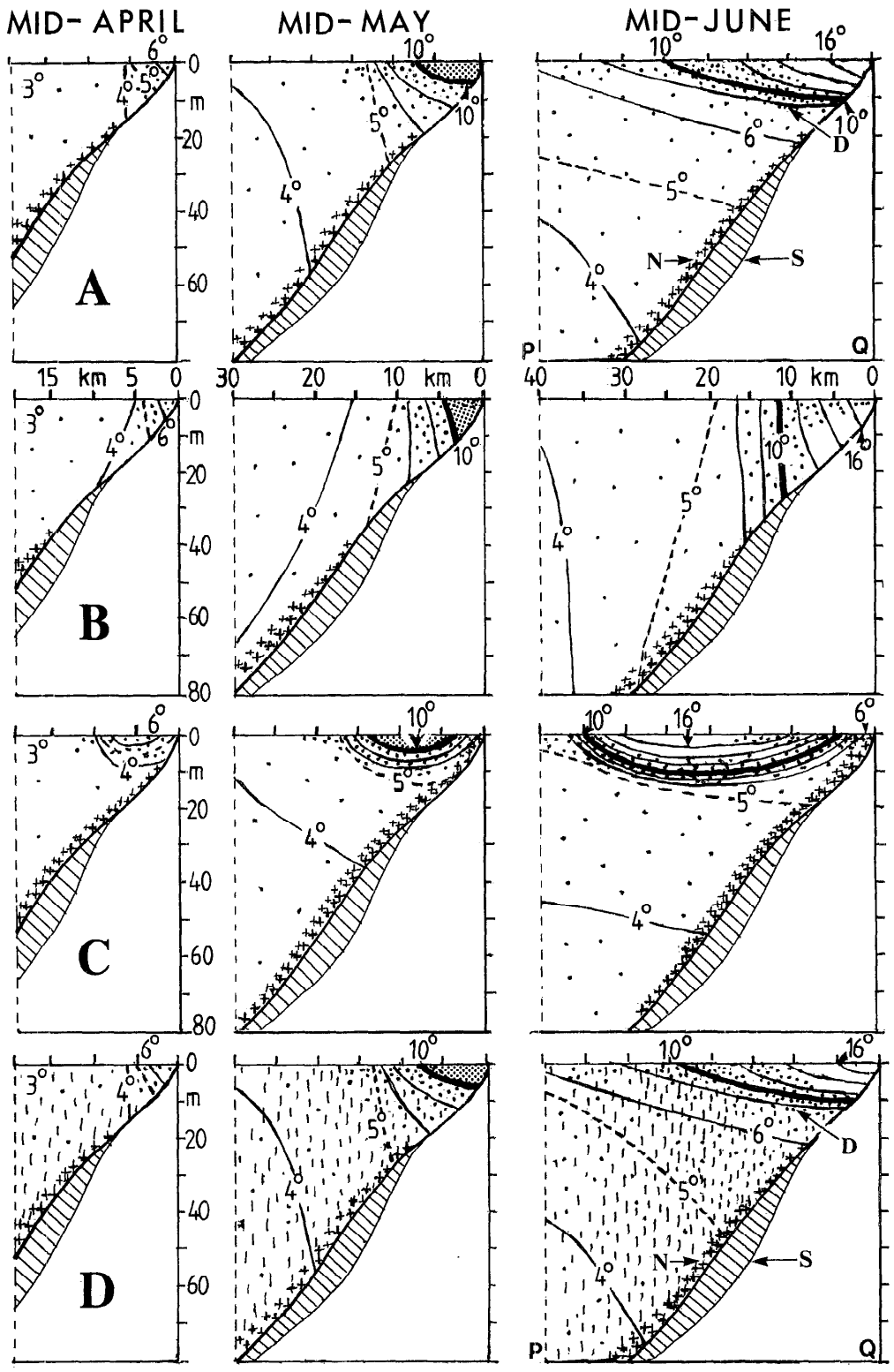
MID-APRIL
MID-MAY
MID-JUNE
A
B
C
D
m
km
N
S
P
Q
D

crosses the area of maximum sediment accumulation (*S*, hatched) and its associated nepheloid layer (*N*, crosses). Random dots represent phytoplankton cells. The stippled upper layer above the 10°C isotherm in the mid-May column marks the temporary trapping of river-derived DOC which forms the dark band (DAB) described previously. Although the DAB starts to form by mid-April, it is too small to be shown in Fig. 13, and (as described earlier) it has dispersed by mid-June.

The unperturbed sequence, represented by row A, is determined by heat flux, moderate wind stress, the Coriolis force, and nutrient uptake and supply. Initial (April) blooming of phytoplankton (mainly diatoms) above the thermocline and inshore of the front is followed by nutrient starvation there in May. It leads to the formation of a deep chlorophyll-maximum layer *D* (tilted with the thermocline). Maximum chlorophyll production is then found near the front, where nutrients are continually entrained from offshore water.

Rows B and C illustrate anticipated perturbations by strong winds from S–SW and from N–NE, respectively, combined with the Coriolis force. Response B is an onshore shift of the isotherms and the plankton-containing water masses. Response C is an offshore shift of the stratified water mass and its inhabitants, leading to onshore upwelling of colder water and, in extreme cases, to the appearance of resuspended particles (crosses) at the surface. Responses B and C are respectively reminiscent of the wedge and lens configurations of front-associated isopycnals observed under different wind regimes by Csanady (1974) and Blanton (1986).

After the winds producing conditions B and C have subsided, the system reverts to condition A or responds to the next perturbation. The resilience of that reversion is strong in April and May, but weaker in June when the inshore–offshore temperature (density) difference is decreasing and whole-basin stratification has begun to set in (Fig. 11). Row D repeats the temperature and phytoplankton distributions of A (i.e. no strong wind effects), but adds an episodic advection of mineral sediment particles (vertical stipples) that have been resuspended elsewhere and advected northward through the PQ section. Occasionally, perturbation D is also imposed on the strong-wind responses B and C, resulting in complex combinations and interactions, yet to be disentangled by field studies.

References

ABBOTT, M. R., AND P. M. ZION. 1985. Satellite observations of phytoplankton variability during an upwelling event. Continental Shelf Res. **4**: 661–680.

ALLENDER, J. H. 1976. Review and appraisal of numerical circulation models for Lake Michigan. Argonne Natl. Lab. Energy Environ. Syst. Div. Rep. ANL/WR-76-6. 104 p.

BELL, G. L., AND B. J. EADIE. 1983. Variations in the distribution of suspended particles during an upwelling event in Lake Michigan in 1980. J. Great Lakes Res. **9**: 559–567.

BENNETT, J. R. 1971. Thermally driven lake currents during the spring and fall transition periods, p. 535–544. *In* Proc. 14th Conf. Great Lakes Res. Int. Assoc. Great Lakes Res.

BLANTON, J. O. 1986. Coastal frontal zones as barriers to offshore fluxes of contaminants. Rapp. P.-V. Cons. Int. Explor. Mer 186, p. 18–30.

BROWN, O. B., AND OTHERS. 1985. Phytoplankton blooming off the US east coast: A satellite description. Science **229**: 163–167.

BUKATA, R. P., J. E. BRUTON, AND J. H. JEROME. 1985. Application of direct measurements of optical parameters to the estimation of lake water quality indicators. Natl. Water Res. Inst. Sci. Ser. No. 140. 35 p. CCIW, Burlington, Ontario.

CHAMBERS, R. L., AND B. J. EADIE. 1981. Nepheloid and suspended particulate matter in southeastern Lake Michigan. Sedimentology **28**: 439–447.

CHURCH, P. E. 1945. The annual temperature cycle of Lake Michigan. 2. Spring warming and summer stationary periods, 1942. Univ. Chicago Inst. Meteorol. Misc. Rep. 18. 100 p.

CSANADY, G. T. 1974. Spring thermocline behavior in Lake Ontario during IFYGL. J. Phys. Oceanogr. **4**: 425–445.

←

Fig. 13. Conjecture-summarizing sketch, in which columns 1–3 represent the anticipated conditions in mid-April, mid-May, and mid-June in transect PQ (Fig. 1a). Rows A–D represent normal (A) and perturbed (B–D) distributions of the spring thermocline, the frontal isotherms, and phytoplankton cells (dots), as described in the text. Q marks the inshore end of the transect near BH; P is 40 km offshore at water depth 90 m; the hatched area marks the maximal accumulation of sediment *S*, above which lies a near-bottom nepheloid layer, *N* (crosses). *D* is a postulated deep chlorophyll-maximum layer.

EDGINGTON, D. N., AND J. A. ROBBINS. 1973. Determination of recent sedimentation rates in Lake Michigan using ^{210}Pb and ^{137}Cs, p. 39–62. *In* Argonne Natl. Lab. Radiol. Environ. Res. Div. Annu. Rep. ANL-8060, part 3.

GORDON, H. R., AND A. Y. MOREL. 1983. Remote assessment of ocean color for interpretation of satellite visible imagery; a review. Lecture Notes Coastal Estuarine Stud. V. 4. Springer.

GOWER, J. F. R. [ED.]. 1981. Oceanography from space. Plenum.

———. 1984. Water colour imaging from space, p. 1–24. *In* Remote sensing of shelf sea hydrodynamics. Elsevier Oceanogr. Ser. 38.

GREAT LAKES BASIN COMMISSION. 1975. Great Lakes Basin framework study, appendices 11 and 12. U.S. Army Corps Eng., North Central Div.

GRIFFITHS, R. W., AND P. F. LINDEN. 1981. The stability of buoyancy-driven coastal currents. Dyn. Atmos. Oceans **5**: 281–306.

HORSTMANN, U. 1983. Distribution patterns of temperature and water colour in the Baltic Sea as recorded in satellite images; indicators for phytoplankton growth. Ber. Inst. Meereskd. Univ. Kiel 106. V. 1. 147 p.

HOVIS, W. A. 1981. The Nimbus-7 Coastal Zone Color Scanner (CZCS) program, p. 213–225. *In* J. R. F. Gower [ed.], Oceanography from space. Plenum.

———. 1984. Practical applications of Nimbus-7 Coastal Zone Color Scanner data, p. 208–211. *In* Recent advances in civil space remote sensing. Proc. Soc. Photo-opt. Instr. Eng. (SPIE). 481.

———, AND OTHERS. 1980. Nimbus-7 Coastal Zone Color Scanner: System description and initial imagery. Science **210**: 60–63.

KUNZE, E., AND T. B. SANFORD. 1984. Observations of near-inertial waves in a front. J. Phys. Oceanogr. **14**: 566–581.

LATHROP, R. G., AND T. M. LILLESAND. 1986. Use of thematic mapper data to assess water quality in Green Bay and central Lake Michigan. Photogram. Eng. Remote Sensing **52**: 671–680.

LINEBACK, J. A., AND D. L. GROSS. 1972. Depositional patterns, facies, and trace element accumulation in the Waukegan Member of the Late Pleistocene Lake Michigan Formation in southern Lake Michigan. Ill. State Geol. Surv. Environ. Geol. Notes 58. 25 p.

MORTIMER, C. H. 1971. Large-scale oscillatory motions and seasonal temperature changes in Lake Michigan and Lake Ontario. Univ. Wis.—Milw. Center for Great Lakes Studies Spec. Rep. 12, parts 1 and 2. 217 p.

———. 1977. Internal waves observed in Lake Ontario during the International Field Year for the Great Lakes (IFYGL) 1972. Univ. Wis.—Milw. Center for Great Lakes Studies Spec. Rep. 32. 122 p.

MURTY, T. S., AND D. B. RAO. 1970. Wind-generated circulations in Lakes Erie, Huron, Michigan, and Superior, p. 927–941. *In* Proc. 13th Conf. Great Lakes Res. Int. Assoc. Great Lakes Res.

NOBLE, V. E., J. C. HUANG, AND J. H. SAYLOR. 1968. Vertical current structure in the Great Lakes. Univ. Mich. Great Lakes Res. Div. Spec. Rep. 37. 94 p.

PINGREE, R. D. 1984. Some applications of remote sensing to studies in the Bay of Biscay, Celtic Sea, and English Channel, p. 287–315. *In* Remote sensing of shelf sea hydrodynamics. Elsevier Oceanogr. Ser. 38.

RAO, D. B., AND B. C. DOUGHTY. 1981. Instability of coastal currents in the Great Lakes. Arch. Meteorol. Geophys. Bioklim. Ser. A **30**: 145–160.

RODGERS, G. K. 1966. The thermal bar in Lake Ontario, spring 1965 and winter 1965–66, p. 369–374. *In* Proc. 9th Conf. Great Lakes Res. Univ. Mich. Great Lakes Res. Div. Publ. 15.

SAYLOR, J. H., J. C. K. HUANG, AND R. O. REID. 1980. Vortex modes in southern Lake Michigan. J. Phys. Oceanogr. **10**: 1814–1823.

SCAVIA, D., AND J. R. BENNETT. 1980. The spring transition period in Lake Ontario—a numerical study of the causes of large biological and chemical gradients. Can. J. Fish. Aquat. Sci. **37**: 823–833.

SMITH, R. C., AND K. S. BAKER. 1982. Oceanic chlorophyll concentrations as determined using Nimbus-7 Coastal Zone Color Scanner imagery. J. Mar. Biol. **66**: 269–279.

STOERMER, E. F. 1968. Nearshore phytoplankton populations in the Grand Haven, Michigan, vicinity during thermal bar conditions, p. 137–150. *In* Proc. 11th Conf. Great Lakes Res. Int. Assoc. Great Lakes Res.

STURM, B. 1982. The atmospheric correction of remotely sensed data and the quantitative determination of suspended matter in marine water surface layers, p. 163–197. *In* A. P. Cracknell [ed.], Remote sensing in meteorology, oceanography and hydrology. Wiley.

SYDOR, M. 1980. Remote sensing of particulate concentrations in water. Appl. Opt. **19**: 2794–2800.

TANIS, F. J. 1984. Phase 2 development of Great Lakes algorithms for Nimbus-7 Coastal Zone Color Scanner. Mich. Environ. Res. Inst. Final Rep. 157900-23-F. Ann Arbor.

TARAPCHAK, S. J., AND E. F. STOERMER. 1976. Phytoplankton of Lake Michigan, p. 114–159. *In* Environmental status of the Lake Michigan region. V. 4. Argonne Natl. Lab. ANL ES-40.

TIKHOMIROV, A. I. 1963. The thermal bar in Lake Ladoga. Bull. All Union Geogr. Soc. **95**: 134–142. [Am. Geophys. Union Transl., Soviet Hydrol. Selected Pap.]

TOPLISS, B. J., AND T. PLATT. 1986. Passive fluorescence and photosynthesis in the ocean: Implications for remote sensing. Deep-Sea Res. **33**: 849–864.

WALTERS, N. M., AND E. H. SCHUMANN. 1985. Detection of silt in coastal waters by Nimbus-7 CZCS, p. 219–225. *In* L. V. Shannon [ed.], South African ocean colour and upwelling experiment. Sea Fish. Res. Inst. Cape Town.

Submitted: 17 November 1986
Accepted: 5 February 1987
Revised: 1 December 1987